AIAA 03–1267

Calculation of Unsteady Transonic Flow by an Euler Method with Small Perturbation Boundary Conditions

C. Gao, S. Luo, F. Liu
Department of Mechanical and Aerospace Engineering
University of California, Irvine, CA 92697-3975

D. M. Schuster
Aeroelasticity Branch
NASA Langley Research Center, Hampton, VA 23681

41st AIAA Aerospace Sciences Meeting and Exhibit
January 6–9, 2003/Reno, NV

Calculation of Unsteady Transonic Flow by an Euler Method with Small Perturbation Boundary Conditions

C. Gao*, S. Luo†, F. Liu‡
Department of Mechanical and Aerospace Engineering
University of California, Irvine, CA 92697-3975

D. M. Schuster§
Aeroelasticity Branch
NASA Langley Research Center, Hampton, VA 23681

This paper demonstrates an efficient numerical method for solving the unsteady Euler equations on stationary Catersian grids. Wall boundary conditions are implemented on non-moving mean wall positions by assuming the airfoil being thin and undergoing small deformation , whereas the full nonlinear Euler equation is used in the field for accurate resolution of shock waves and vorticity, and the mean angle of attack of the body can be large. The method does not require the generation of moving body-fitted grids and thus can be easily deployed in any fluid-structure interaction problem involving relatively small deformation of a thin body. The first-order wall boundary conditions is used in solving the full Euler equations, and the results are compared with the Euler solutions using the exact boundary conditions and known experimental data. It is shown that the first-order boundary conditions are adequate to represent airfoils of typical thicknesses with small deformation for both steady and unsteady calculations.

I. Nomenclature

c	Airfoil chord
C_{dw}	Wave drag coefficient
C_l	Lift coefficient
C_m	Moment coefficient around quarter chord, positive nose up
C_p	Pressure coefficient
C_p^*	Critical pressure coefficient
$(\mathbf{e}_x, \mathbf{e}_y)$	Unit vectors in (x, y) directions
E	Total specific energy
$F(t, x)$	Instantaneous upper-surface of airfoil
$G(t, x)$	Instantaneous lower-surface of airfoil
$f(x)$	Mean upper-surface of airfoil
$g(x)$	Mean lower-surface of airfoil
$\mathbf{G}$	Euler flux vector
H	Total specific enthalpy
(i, j)	Grid point index
κ	Reduced frequency
M_∞	Freestream Mach number
N_{step}	Number of even real-time steps in one period of oscillation
$\mathbf{n}$	Outer normal vector to cell surface
n	Real time level
p	Pressure
Re	Reynolds number based on chord length
$\mathbf{q}$	Velocity vector of fluid particle
$\mathbf{q}_b$	Velocity vector of the surface of control volume
R	Flux residual
R^*	Modified residual
S	Surface of control volume
t	Real time
t^*	Pseudo-time
U_∞	Free stream velocity
u, v	x and y velocity components of fluid particle
u_b, v_b	x and y components of grid velocity
V	Control volume
$\mathbf{W}$	Euler conservative flow variable
x, y	Cartesian coordinates
x_0	x-coordinate of the pivot point of airfoil pitching
α	Instantaneous angle of attack, deg
α_m	Mean angle of attack, deg
α_1	Instantaneous increment of angle of attack, deg
α_0	Amplitude of the pitching oscillation
Δt	Real-time step
$\Delta x, \Delta y$	Grid spacing in (x, y) directions
γ	Ratio of specific heats
ρ	Air density
ω	Angular frequency

*Visiting Associate Researcher. Associate Professor, Northwestern Polytechnical University, Xi'an, China.

†Researcher.

‡Associate Professor. Senior Member AIAA.

§Senior Research Engineer. Associate Fellow AIAA

II. Introduction

Computational Fluid Dynamics (CFD) has proven to be a useful tool for the simulation and prediction of buffet, flutter, and Limit Cycle Oscillation (LCO) phenomena of aeroelastic systems. Methods ranging from the linear doublet-lattice method[1] to methods that solve the Euler and the Navier-Stokes equations have been developed.[2–7] Despite its limit in handling transonic and other nonlinear flows, the linear doublet lattice method has been and is still the workhorse for actual design analysis in industry because of its efficiency in computer time and, perhaps equally important, the ease in setting up the computational problem. The Reynolds-Averaged-Navier-Stokes (RANS) methods encompass the most complete flow model short of Large-Eddy-Simulations (LES) or Direct-Numerical-Simulations (DNS). However, RANS simulations for aeroelasticity problems at present demand computational resources beyond those tolerable in a design environment. In addition, their usefulness is limited by uncertainties in turbulence modeling, grid resolution, and numerical damping effects;[6,7] difficulties in grid generation and the transfer of displacements and aerodynamic forces between the structural and aerodynamic grids; and lack of fast and robust algorithms for deforming grids needed in the unsteady computations. In between the above two extremes, methods based on the various forms of the potential flow equation with boundary-layer corrections have shown good results for flutter simulations without the use of large computational resources and with less human work in setting up the computational problem including grid generation. Among such methods, the CAP-TSD[8–10] code is widely known and used. The CAP-TSD code has many advantages over a full-fledged RANS code. These include 1) ease in generating a grid; 2) no need to do complex interpolation between the structural and CFD grids; 3) no need to have a moving grid; 4) less demand on CPU time and memory.

Despite the use of vortex and entropy corrections, the potential flow assumption in CAP-TSD limits its applicability to irrotational flows with weak shocks. Advances in computer speed and maturity of algorithms for the Euler equations have made the solution of the Euler equations a rather dependable and routine tool. Although the Euler equations can not account for the viscous effects in the boundary layer, it is capable of resolving strong shocks and transporting vortices correctly. Due to the requirement of large computing resources by a Navier-Stokes code and also unresolved issues regarding accuracy of current numerical algorithms for the Navier-Stokes equations, the Euler equations strike a good balance between completeness of the flow model and computational efficiency. In order to retain the ease in setting up a computational grid as in the CAP-TSD code, this paper investigates the use of the boundary conditions based on the assumption of thin airfoil with small deformations.

The unsteady Euler equations and a fully implicit time-accurate scheme are briefly reviewed.[11] Details of the mathematical formulation of the approximate boundary conditions are presented along with their implementation in the finite-volume codes, FLO52 and NS83. The former is a well-established Euler code for steady flows,[12] and the latter is an established finite-volume code for the unsteady Euler/Navier-Stokes equations.[13] Numerical examples are given and the results are compared with those obtained by the original FLO52 and the published experimental data. Discussions and conclusions are finally drawn.

III. Euler Equations and Time-Accurate Scheme

Consider a moving and possibly deforming control volume (computational cell) V in two dimensions whose boundary S moves at velocity (u_b, v_b). The two-dimensional unsteady Euler equations in conservative integral form in the Cartesian coordinate system (x, y) for such a control volume are

$$\frac{\partial}{\partial t}\int_V \mathbf{W} dV + \int_S \mathbf{G}\cdot\mathbf{n} dS = 0 \tag{1}$$

where

$$\mathbf{W} = \begin{bmatrix} \rho \\ \rho u \\ \rho v \\ \rho E \end{bmatrix} \tag{2}$$

$$\mathbf{G} = \begin{bmatrix} \rho(\mathbf{q}-\mathbf{q}_b) \\ \rho u(\mathbf{q}-\mathbf{q}_b) + p\mathbf{e}_x \\ \rho v(\mathbf{q}-\mathbf{q}_b) + p\mathbf{e}_y \\ \rho E(\mathbf{q}-\mathbf{q}_b) + p(u\mathbf{e}_x + v\mathbf{e}_y) \end{bmatrix} \tag{3}$$

$$\mathbf{q} = u\mathbf{e}_x + v\mathbf{e}_y \tag{4}$$

$$\mathbf{q}_b = u_b\mathbf{e}_x + v_b\mathbf{e}_y \tag{5}$$

$$E = \frac{1}{\gamma-1}\frac{p}{\rho} + \frac{1}{2}(u^2+v^2) \tag{6}$$

Applying (1) to each cell in the mesh we obtain a set of ordinary differential equations of the form

$$\frac{d}{dt}(\mathbf{W}_{i,j}V_{i,j}) + \mathbf{R}(\mathbf{W}_{i,j}) = 0 \tag{7}$$

where $V_{i,j}$ is the volume of the i,j cell and the residual $\mathbf{R}(\mathbf{W}_{i,j})$ is obtained by evaluating the flux integral in (1). Following Jameson,[11] we approximate the $\frac{d}{dt}$ operator by an implicit backward difference formula of second-order accuracy in the following form (dropping the subscripts i,j for clarity)

$$\frac{3}{2\Delta t}[\mathbf{W}^{n+1}V^{n+1}] - \frac{2}{\Delta t}[\mathbf{W}^{n}V^{n}] + \frac{1}{2\Delta t}[\mathbf{W}^{n-1}V^{n-1}] + \mathbf{R}(\mathbf{W}^{n+1}) = 0 \quad (8)$$

Eqn. (8) can be solved for $\mathbf{W}^{n+1}$ at each time step by solving the following steady-state problem in a pseudo time t^*.

$$\frac{d\mathbf{W}}{dt^*} + \mathbf{R}^*(\mathbf{W}) = 0 \quad (9)$$

where

$$\mathbf{R}^*(\mathbf{W}) = \mathbf{R}(\mathbf{W}) + \frac{3}{2\Delta t}(\mathbf{W}V^{n+1}) - \frac{2}{\Delta t}(\mathbf{W}^{n}V^{n}) + \frac{1}{2\Delta t}(\mathbf{W}^{n-1}V^{n-1}) \quad (10)$$

Eqn. (9) is solved by an explicit time-marching scheme in t^* for which the local time stepping, residual smoothing, and multigrid techniques[12] can be used to accelerate convergence to a steady state.

In the present approximate method, the grid does not change with the time even for unsteady flow calculations. Thus, in the above equations the cell volume V satisfies $V^{n+1} = V^n = V^{n-1} = V$, and $\mathbf{q}_b = 0$.

IV. Approximate Boundary Conditions

A thin airfoil slightly moving or deforming about its mean position is considered. The mean position of the airfoil chord lies on the horizontal axis x of the coordinate system between $x = 0$ and $x = 1$. The velocity of the incoming uniform free stream makes an angle α_m with the x axis. In the present paper, the airfoil is assumed to be of rigid shape but performs an oscillating motion around a fixed point on its chord line at $x = x_0$. The shape of the airfoil is described by $y = f(x)$ and $g(x)$ for its upper and lower surfaces, respectively. The instantaneous position of the airfoil is described by $y = F(t,x)$ and $y = G(t,x)$ for the upper and lower surfaces, respectively. The flow is assumed inviscid. The boundary conditions on the upper surface of the airfoil at an instant t is

$$v(t,x,F) = u(t,x,F)F_x + F_t \quad (11)$$

where the subscripts, x and t denote the partial derivatives with respect to x and t, respectively. Under the assumption, $|F| \ll 1$, the first-order approximation of (11) on the x axis is

$$v(t,x,0) = u(t,x,0)F_x + F_t + O(F) \quad (12)$$

where $O(F)$ represents terms of the same order of magnitude as F or higher.

The boundary condition on the lower surface is treated similarly. The mean position of the leading edge of the airfoil is chosen as the origin of the coordinate system. If the leading edge is blunt, the boundary condition there is replaced by

$$u = 0 \quad (13)$$

At the sharp trailing edge of the airfoil, the pressures on the upper and lower surfaces should be equal to each other. In supercritical flow with adiabatic shock waves, the velocities and densities at the sharp trailing edge on the upper and lower surfaces may not be equal to each other. It is known that the Kutta condition at the sharp trailing edge is satisfied automatically in Euler calculations.

There are altogether four independent variables in the Euler equations (1), e.g. ρ, u, v and p. In addition to the boundary conditions of the velocity given above, more conditions are needed on the airfoil surfaces. The momentum differential equation in the outward normal direction $\mathbf{n}$ is also used, which gives

$$\mathbf{n} \cdot [\frac{\partial \mathbf{q}}{\partial t} + (\mathbf{q} \cdot \nabla)\mathbf{q}] = \mathbf{n} \cdot (-\frac{\nabla p}{\rho}) \quad (14)$$

On the upper surface of the airfoil, $y = F(t,x)$, the above equation becomes

$$p_y(t,x,F) = F_x p_x(t,x,F) - \rho(t,x,F)[F_{tt} + 2F_{tx}u(t,x,F) + F_{xx}u^2(t,x,F)] \quad (15)$$

The first-order approximation of the above equation is

$$p_y(t,x,0) = F_x p_x(t,x,0) - \rho(t,x,0)[F_{tt} + 2F_{tx}u(t,x,0) + F_{xx}u^2(t,x,0)] + O(F) \quad (16)$$

The corresponding equations on the lower surface of the airfoil are similarly derived.

In this paper, a rigid airfoil performing pitching oscillation about a point at $x = x_0$ on its mean chord is considered as an example. The instantaneous angle of the pitching rotation from the mean position is $\alpha_1(t)$, positive in clockwise direction. Given $f(x)$, the instantaneous ordinate of the upper surface, $F(t,x)$, is expressed implicitly as follows.

$$F\cos\alpha_1 + (x - x_0)\sin\alpha_1 = f\left(x_0 + (x - x_0)\cos\alpha_1 - F\sin\alpha_1\right) \quad (17)$$

where the expression $x_0 + (x - x_0)\cos\alpha_1 - F\sin\alpha_1$ in the first pair of parentheses on the right-hand-side of the equation is the argument of the function $f(x)$.

The five derivatives of $F(t,x)$ used in the first-order approximate boundary conditions can be evaluated exactly by the following set of equations.

$$\begin{aligned}
F_x &= \frac{f'\cos\alpha_1 - \sin\alpha_1}{\cos\alpha_1 + f'\sin\alpha_1} \\
F_{xx} &= \frac{f''(\cos\alpha_1 - F_x\sin\alpha_1)}{(\cos\alpha_1 + f'\sin\alpha_1)^2} \\
F_t &= \alpha_1'[F(\sin\alpha_1 - f'\cos\alpha_1) \\
&\quad -(x-x_0)(\cos\alpha_1 + f'\sin\alpha_1)] \\
&\quad /(\cos\alpha_1 + f'\sin\alpha_1) \\
F_{tx} &= -\{f''[\alpha_1'(x-x_0)\sin\alpha_1 + F_t\sin\alpha_1 \\
&\quad +F\alpha_1'\cos\alpha_1] + \alpha_1'(1+f'^2)\} \\
&\quad /(\cos\alpha_1 + f'\sin\alpha_1)^2 \\
F_{tt} &= \alpha_1''[F(\sin\alpha_1 - f'\cos\alpha_1) \\
&\quad -(x-x_0)(\cos\alpha_1 + f'\sin\alpha_1)] \\
&\quad /(\cos\alpha_1 + f'\sin\alpha_1) \\
&\quad +\{\alpha_1'F_t[(1-f'^2)\sin\alpha_1\cos\alpha_1 \\
&\quad -f'\cos 2\alpha_1 + Ff''\sin\alpha_1] \\
&\quad +\alpha_1'^2F[1+f'^2+f''(x-x_0)\sin\alpha_1 \\
&\quad +Ff''\cos\alpha_1]\}/(\cos\alpha_1 + f'\sin\alpha_1)^2
\end{aligned} \tag{18}$$

where the $'$ denotes differentiation of $f(x)$ and $\alpha(t)$ with respect to x and t, respectively.

In the present approximation, $|\alpha_1| \ll 1$ and $|F| \ll 1$, and the computational grid does not vary with time. The argument of the function f in (17) can be approximated as follows.

$$(x-x_0)\cos\alpha_1 - F\sin\alpha_1 + x_0 = x + O(F^2) \tag{19}$$

The implicit expression for F, (17) can be simplified into an explicit one.

$$F = \frac{f(x)}{\cos\alpha_1} - (x-x_0)\tan\alpha_1 + O(F^2) \tag{20}$$

Given this explicit expression, the five derivatives of $F(t,x)$ derived exactly above can be easily re-evaluated. The deviations of the approximate results from the exact ones are all of the order $O(F^3)$.

$$\begin{aligned}
F_x &= f' - \tan\alpha_1 + O(F^3) \\
F_{xx} &= f'' + O(F^3) \\
F_t &= -\alpha_1'(x-x_0)\sec^2\alpha_1 + O(F^3) \\
F_{tx} &= -\alpha_1'\sec^2\alpha_1 + O(F^3) \\
F_{tt} &= -(x-x_0)\sec^2\alpha_1(\alpha_1'' + 2\alpha_1'^2\tan\alpha_1) + O(F^3)
\end{aligned} \tag{21}$$

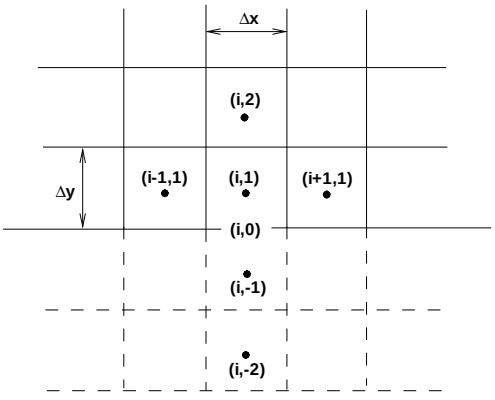

Fig. 1 Grids and fictitious grids.

It will be shown below that using these approximate derivative expressions to calculate the aerodynamic force causes negligible errors in a numerical example.

For steady flow, $F(t,x) = f(x)$, $\alpha_1 = 0$ and $\alpha = \alpha_m$ in the above equations.

V. Numerical Implementation of the Boundary Conditions

Since the boundary of the airfoil is put on the x axis, $y = 0$, the computational grids can be taken to be rectilinear and parallel to the coordinate axes, x and y. Two fictitious grid layers extending from the airfoil boundary outward are used in the finite volume method in order to calculate the flux vector $\mathbf{G}$ and the second- and fourth-order artificial dissipation terms.

Figure 1 shows the two grid layers above the upper surface of $y = 0$ and the two fictitious grid layers extended from above. In the y direction, the two grids upward from $y = 0$ are named as 1 and 2, and the two grids downward from $y = 0$ are named as -1 and -2. The upper surface $y = 0$ is denoted by 0. In the x direction, the three consecutive grids are denoted by $i-1$, i, and $i+1$. Δx and Δy are the grid intervals in the x and y directions, respectively. All the following expressions are derived for the same pseudo-time level, and thus the independent variable, t^*, is dropped.

The density at the fictitious grid centers are evaluated by the linear extrapolation from the above.

$$\rho_{i,-1} = 2\rho_{i,1} - \rho_{i,2} \tag{22}$$

$$\rho_{i,-2} = 2\rho_{i,-1} - \rho_{i,1} \tag{23}$$

The products of ρ and u at the fictitious grid centers are evaluated by the same linear extrapolation formula as those for ρ. Then the values of u at the fictitious

grid centers are determined as the quotient of the local values of (ρu) and u. The value of u on the upper surface, $y = 0$ is

$$u_{i,0} = \frac{1}{2}(u_{i,-1} + u_{i,1}) \tag{24}$$

Using the boundary condition (12), the value of v on the upper surface, $y = 0$ is

$$v_{i,0} = F_{ti} + F_{xi} u_{i,0} \tag{25}$$

The values of v at the fictitious grid centers are evaluated as

$$v_{i,-1} = -v_{i,1} + 2v_{i,0} \tag{26}$$

$$v_{i,-2} = -v_{i,2} + 2v_{i,0} \tag{27}$$

The pressure at the fictitious grid centers are evaluated by using the boundary equation (16).

$$p_{i,-1} = p_{i,-2} = max[(p_{i,1} - p_{y0}\Delta y), 0] \tag{28}$$

where

$$\begin{aligned} p_{y0} &= F_{xi} p_{x0} - \rho_{i,0}(F_{tti} + 2F_{txi} u_{i,0}) \\ &\quad -F_{xxi}(\rho_{i,0} u_{i,0})^2/\rho_{i,0} && (29) \\ p_{x0} &= (p_{i+1,1} - p_{i-1,1})/(2\Delta x) && (30) \\ \rho_{i,0} u_{i,0} &= (\rho_{i,-1} u_{i,-1} + \rho_{i,1} u_{i,1})/2 && (31) \\ \rho_{i,0} &= (\rho_{i,-1} + \rho_{i,1})/2 && (32) \end{aligned}$$

Once the values of ρ, u, v, and p at the fictitious grid centers and on the boundary, $y = 0$, are determined, the other flow parameters can be evaluated by their definitions. The fictitious grid values of ρE are calculated as follows.

$$\begin{aligned} \rho_{i,-1} E_{i,-1} &= \frac{p_{i,-1}}{\gamma - 1} + \frac{(\rho_{i,-1} u_{i,-1})^2 + (\rho_{i,-1} v_{i,-1})^2}{2\rho_{i,-1}} \\ \rho_{i,-2} E_{i,-2} &= \rho_{i,-1} E_{i,-1} && (33) \end{aligned}$$

For steady flow, $F_{ti} = F_{txi} = F_{tti} = 0$ in the above equations, and an alternative is to use the constant total enthalpy condition to determine ρE of the fictitious grid points, i.e.

$$\rho_{i,-1} E_{i,-1} = \frac{\rho_{i,-1}}{\rho_{i,1}}(\rho_{i,1} E_{i,1} + p_{i,1}) - p_{i,-1} \tag{34}$$

VI. Results and Discussions

A. Steady Flows

The steady inviscid compressible flows about three airfoils, NACA 0006, NACA 0012, and NACA 0015 are computed by FLO52 and the present approximate method at the Mach numbers $M_\infty = 0.8$ and 0.725, and the angles of attack, α, from 0 to 8 degrees. FLO52 uses body-conforming curvilinear grids generated by conformal mapping. An O-type grids with 161×33 grid points are used for the benchmark calculations in this paper. The rectilinear grids used in the present approximate calculations consists of 141×67 grid points. For both grids, there are 160 grid points on the airfoil surface, and the distances between the far field boundaries and the airfoil are about $25\times$ (chord length). Both grids are non-uniformly spaced so that more grid points are located in the neighborhood of the airfoil. Furthermore, grid points are also clustered near the leading and trailing edges. The criterion for the convergence of the computations is that the maximum magnitude of the residuals be reduced by more than four orders of magnitude. To achieve this criterion it takes about $1,000$ steps of calculations with the present method. The multigrid algorithm in FLO52 is not used in the present calculations.

Figure 2 shows the comparisons of the pressure distributions over the airfoil NACA 0015 at $M_\infty = 0.8$ and $\alpha = 0, 4, 8$ degrees with those obtained by FLO52. The pressure distributions of the present approximate calculations are evaluated on the chord line, $y = 0$, instead of on the exact upper and lower surfaces. Numerical experiments show that the former method yields results closer to the solutions of FLO52. It is seen that the present results agree well with those obtained by the FLO52 even for the airfoil with a thickness ratio as large as 15% and angle of attack as large as 8 degrees. It is noted that when α is moderate and large, there appears a small bump in c_p on the upper surface in the region from $x = 0.05$ to $x = 0.1$ in the present solutions. In the above approximate calculations, the constant total enthalpy equation (34) is used to determine the fictitious values of ρE. If Eqn. (33) is used instead, this bump becomes slightly larger and the local shock wave moves slightly downstream as shown in Figure 3 for the case $\alpha = 4$ degrees.

Figure 4 gives the comparisons of the computed lift coefficient, c_l, wave drag coefficient, c_{dw} and pitching moment coefficient about quarter chord, c_m, vs. α from 0 to 8 degrees at $M_\infty = 0.8$ with the FLO52 results. The relative errors of c_l, c_{dw}, and c_m are in general within 10 %.

Figure 5 shows the comparisons of the pressure distributions over the airfoil NACA 0012 at $M_\infty = 0.8$ and $\alpha = 0, 4$ degrees with those obtained by FLO52. Figure 6 gives the comparisons of c_l, c_{dw} and c_m vs. α from 0 to 4 degrees, with the FLO52 results.

Figure 7 shows the comparisons of the pressure distributions over the airfoil NACA 0006 at $M_\infty = 0.8$ and $\alpha = 0, 4$ degrees with those obtained by FLO52. Figure 8 gives the comparisons of c_l, c_{dw}, and c_m vs. α from 0 to 4 degrees. Both Figures 5 and 7 show

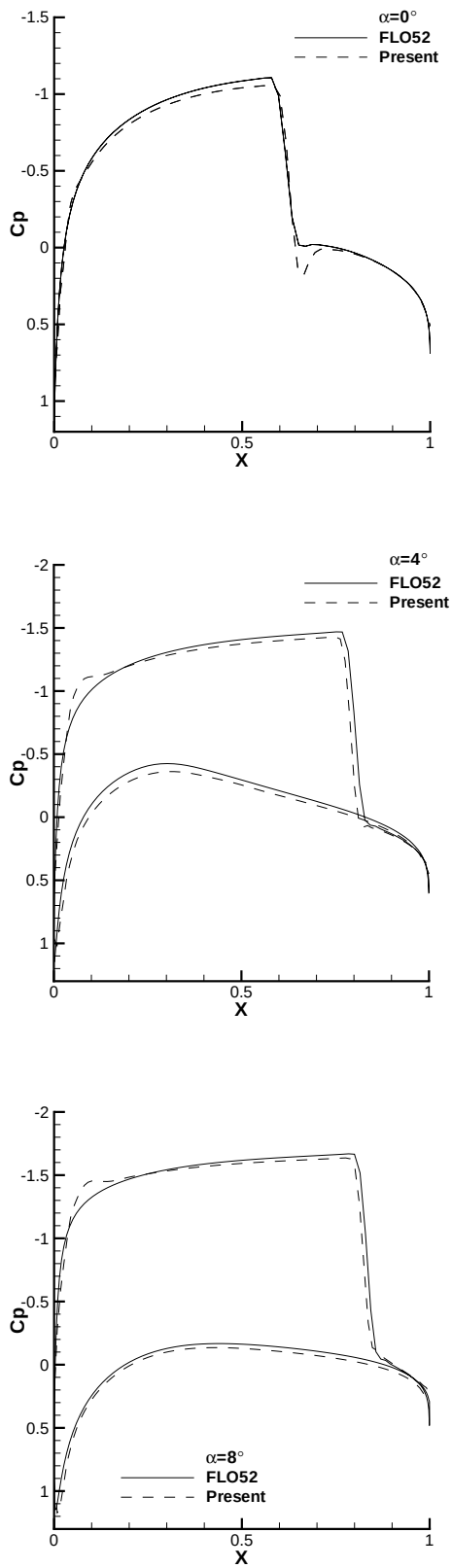

Fig. 2 Comparison of pressure distributions, NACA 0015, $M_\infty = 0.8$, $\alpha = 0, 4, 8$ deg.

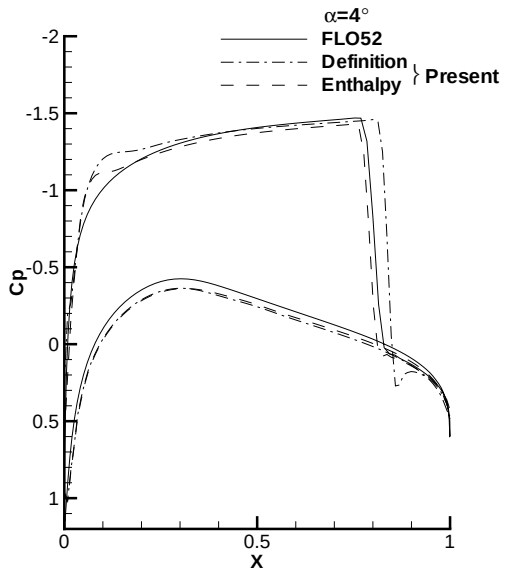

Fig. 3 Comparison of pressure distributions, NACA 0015, $M_\infty = 0.8$, $\alpha = 4$ deg.

that the present method predicts shock waves that are noticeably forward compared to the results by FLO52 at higher angles of attack. This may be indicative of a dissipative-like mechanism that effectively moves the shock forward in an inviscid conservative code.

The steady inviscid compressible flows around the above three airfoils at $M_\infty = 0.725$ and $\alpha = 0 \sim 8$ degrees are also computed by the present approximate method and FLO52. The results are not included in this paper due to space limitation but show similar comparative qualities as in the case of $M_\infty = 0.8$. In all the numerical examples, it is seen that the present approximate method in general yields quite accurate pressure distributions over the airfoils. They are excellent when the angle of attack is small. When the angle of attack is moderate and the thickness ratio is large, there appears a small bump around 10% of chord length from the leading edge on the suction side. Numerical experiments show that the constant total enthalpy condition given by Eqn. (34) usually gives slightly better results than the condition using Eqn. (33). Preliminary numerical experiments, which are not included in the present paper, indicate that an adjustment of the present grids around the airfoil leading edge so that the exact boundary condition (13) is explicitly embedded into the finite volume schemes may improve the present results.

B. Unsteady Flows

The present approximate method is used to calculate the flow over an NACA 0012 airfoil pitching

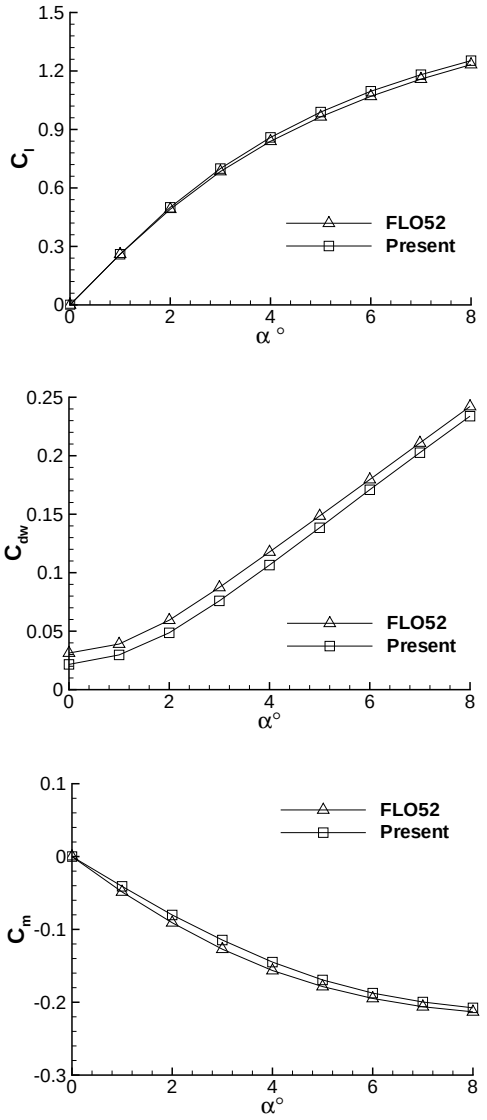

Fig. 4 Comparison of c_l, c_{dw} and c_m, NACA 0015, $M_\infty = 0.8$, $\alpha = 0 \sim 8$ deg.

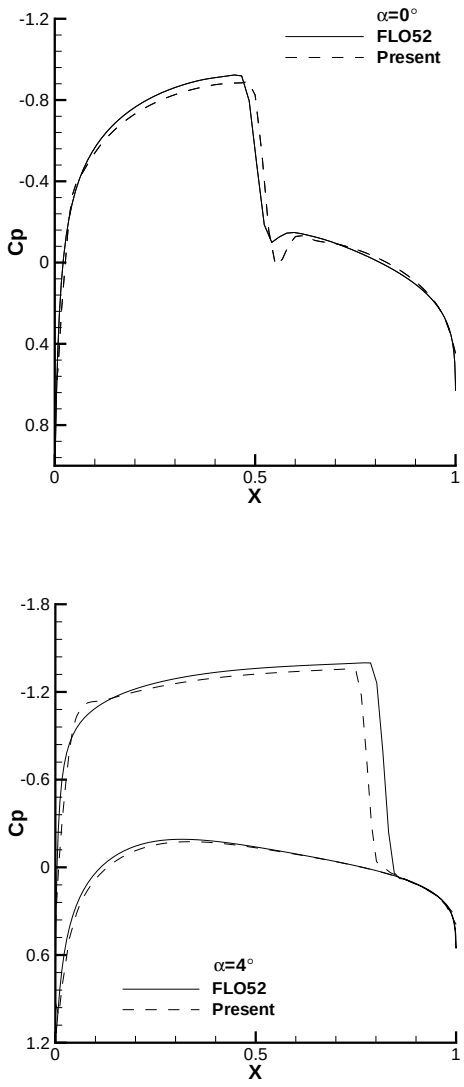

Fig. 5 Comparison of pressure distributions, NACA 0012, $M_\infty = 0.8$, $\alpha = 0, 4$ deg.

around its quarter-chord point. Experimental data were provided by Landon.[14] The pitching motion of the airfoil is described by the following equation.

$$\alpha(t) = \alpha_m + \alpha_0 \sin \omega t \tag{35}$$

where ω, α_m and α_0 are constants. The angular frequency ω is related to the reduced frequency defined as

$$\kappa = \frac{\omega c}{2U_\infty} \tag{36}$$

The rectilinear grids used in the unsteady-flow calculations are the same as that used in the above steady-flow computations. The criterion for the convergence of the pseudo-time computations is that the maximum magnitude of the residuals be reduced by more than four orders of magnitude. To satisfy this criterion, the number of the pseudo-time steps is usually 150. The calculations start from the uniform flow of velocity U_∞ as an initial solution. After three real-time cycles of the airfoil motion an essentially periodic solution is obtained. In this paper six cycles of motion are used to ensure the computed results to be periodic.

Before comparing the approximate boundary-condition results with the experimental data, there are two questions to be answered by numerical experiments. The first question is how many real-time steps in one complete period of the airfoil oscillation, N_{step}, are adequate to obtain the time-accurate lift coefficient

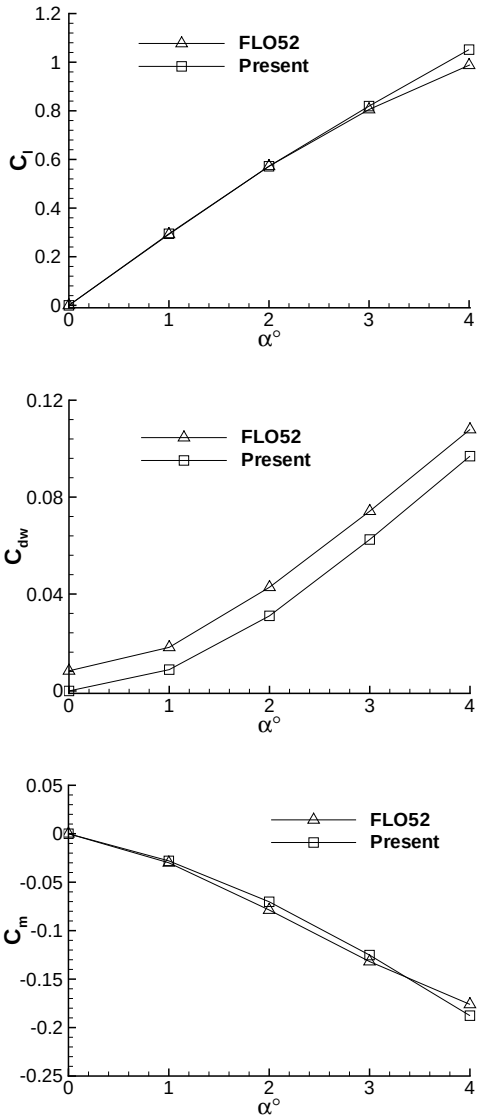

Fig. 6 Comparison of c_l, c_{dw}, and c_m, NACA 0012, $M_\infty = 0.8$, $\alpha = 0 \sim 4$ deg.

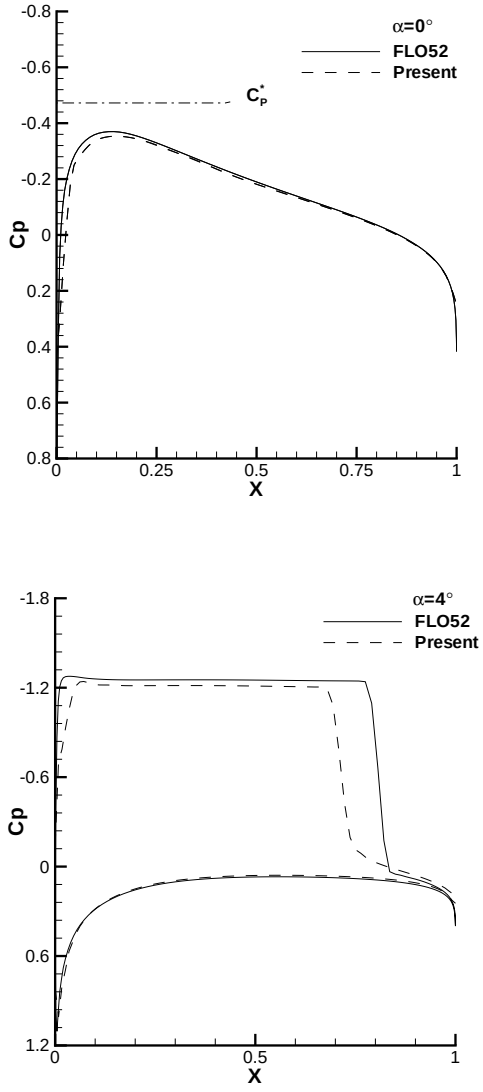

Fig. 7 Comparison of pressure distributions, NACA 0006, $M_\infty = 0.8$, $\alpha = 0, 4$ deg.

$C_l(t)$ and pitching moment coefficient $C_m(t)$ about the quarter-chord point. The upper of Figure 9 gives the comparison of $C_l(\alpha)$ within one period of oscillation calculated with $N_{step} = 32$ and 64 for the airfoil NACA 0012 at $M_\infty = 0.755, \alpha_m = 0.016\,\text{deg}, \alpha_0 = 2.51\,\text{deg}$, and $\kappa = 0.0814$. The lower of Figure 9 gives the corresponding comparison of $C_m(\alpha)$ at the same conditions. It is seen that the results calculated with $N_{step} = 32$ and $N_{step} = 64$ agree well with each other. Therefore, N_{step} is taken as as 32 in the present investigation.

The second question is how much error is induced when the accurate expressions of (18) for the derivatives F_x, F_{xx}, F_t, F_{tx}, and F_{tt} are replaced by the corresponding approximate expressions (21). Figure 10 compares $C_l(\alpha)$ and $C_m(\alpha)$ within one period of oscillation calculated by using the two set of expressions for the NACA 0012 airfoil at $M_\infty = 0.8, \alpha_m = 0\,\text{deg}, \alpha_0 = 1\,\text{deg}$, $\kappa = 0.1$, and $N_{step} = 32$. The results calculated by the approximate expressions for the five derivatives of $F(t, x)$ coincide with those calculated by the corresponding exact expressions. Therefore, the approximate expressions (21) are used in the following computations.

The present approximate method is verified by comparing with the experimental results of Landon.[14] The AGARD CT case 5 of Reference 14 is studied. The airfoil is an NACA 0012 pitching at the free stream Mach number $M_\infty = 0.755, \alpha_m = 0.016\,\text{deg}, \alpha_0 = 2.51\,\text{deg}, \kappa = 0.0814$. The experimental $Re = 5.5 \times 10^6$.

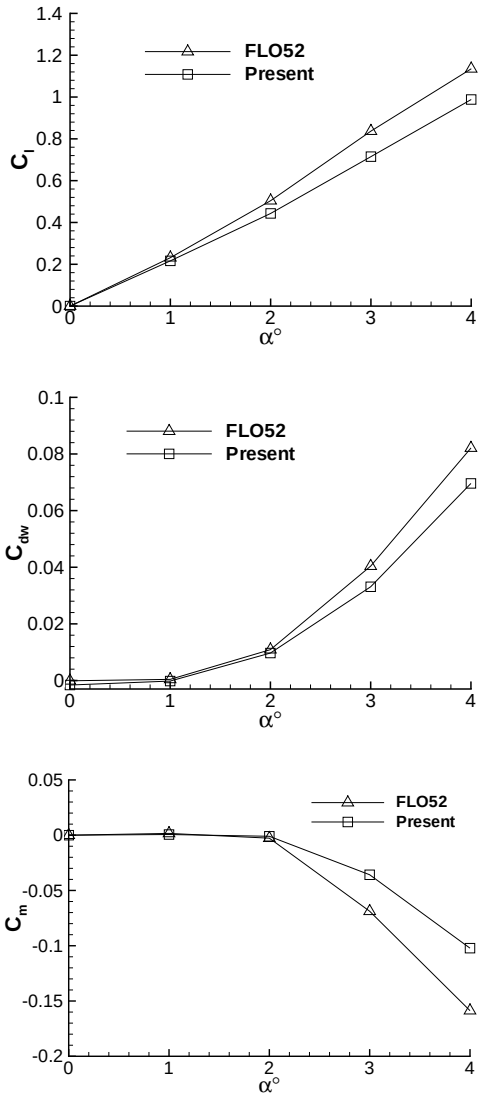

Fig. 8 Comparison of c_l, c_{dw} and c_m, NACA 0006, $M_\infty = 0.8$, $\alpha = 0 \sim 4$ deg.

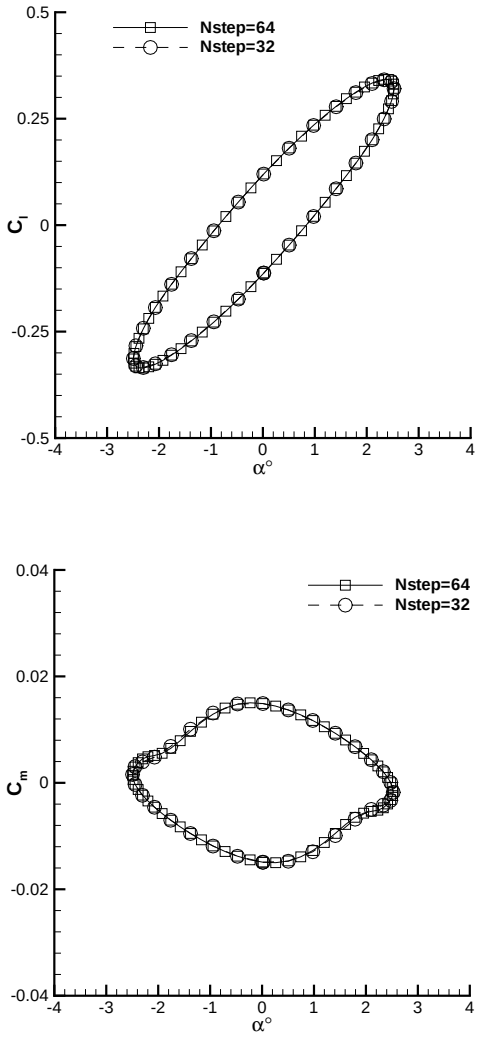

Fig. 9 Comparison of lift and moment coefficients computed with $N_{step} = 32$ and $N_{step} = 64$, NACA 0012, $M_\infty = 0.755$, $\alpha_m = 0.016\,\text{deg}$, $\alpha_0 = 2.51\,\text{deg}$, $\kappa = 0.0814$,

The Comparisons of the present inviscid computations and the experimental data of the instantaneous lift and moment coefficients vs. the instantaneous angle of attack are presented in Figure 11. The computed instantaneous pressure distributions by the present approximate boundary conditions at the eight phase angles during the sixth cycle of motion are compared with the experimental data in Figure 12. The eight phase angles are $25.3, 67.8, 127.4, 168.4, 210.3, 255.1, 306.6$, and 347.2 degrees. The computed pressure distributions by the present approximate method agree quite well with the experimental data.

The time variation of the computed and experimental data of the surface pressure distributions can be expressed in terms of their Fourier components. Figure 13 shows the comparison between the present approximate solutions and the experimental unsteady pressure for the real and imaginary parts of the first three Fourier modes. It is seen that a good agreement is obtained between the results obtained by the present approximate method and the experimental data.

Batina[15] computed the Euler solutions with full boundary conditions on an unstructured body-fitted grid and compared his solutions with the same experimental data as we have done here. His computed results have qualitatively the same degree of agreement with the experimental data as do the computed results by the present approximate method.

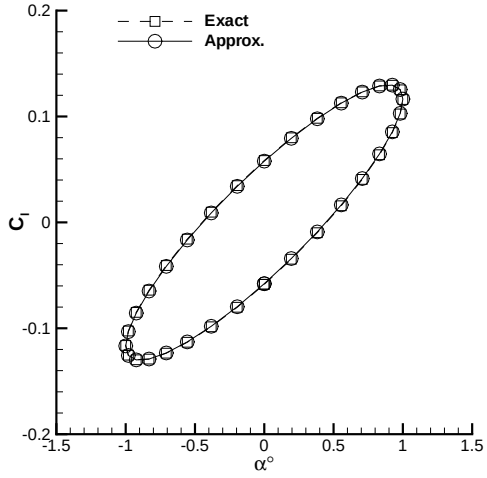

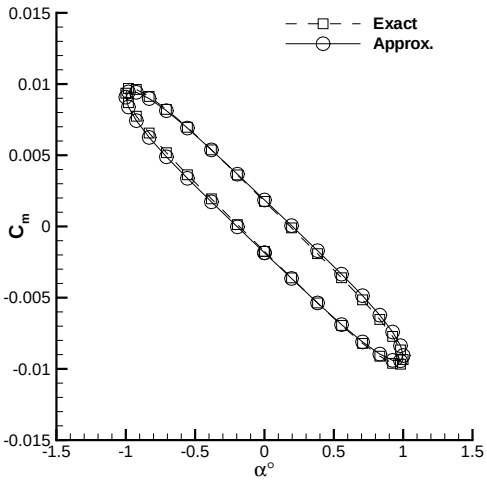

Fig. 10 Comparison of lift and moment coefficients computed with the exact formulae (18) and the approximate formulae (21), NACA 0012, $M_\infty = 0.8$, $\alpha_m = 0$, $\alpha_0 = 1\,\mathrm{deg}$, $\kappa = 0.1$.

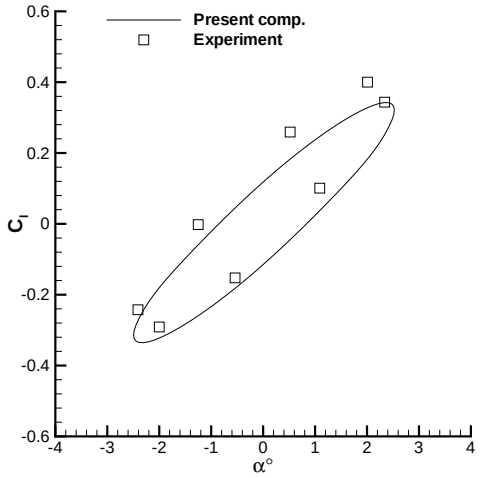

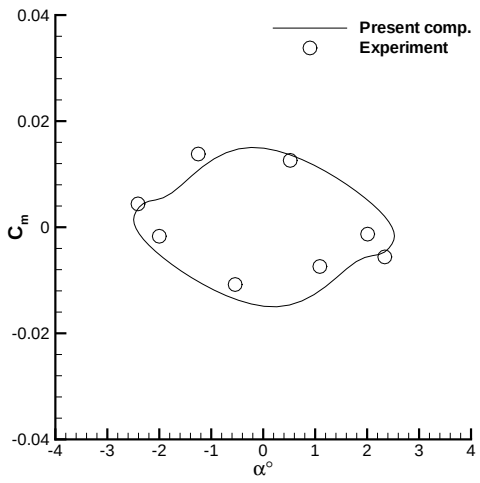

Fig. 11 Comparison of lift and moment coefficients between present computation and experiment, NACA 0012, $M_\infty = 0.755$, $\alpha_m = 0.016\,\mathrm{deg}$, $\alpha_0 = 2.51\,\mathrm{deg}$, $\kappa = 0.0814$.

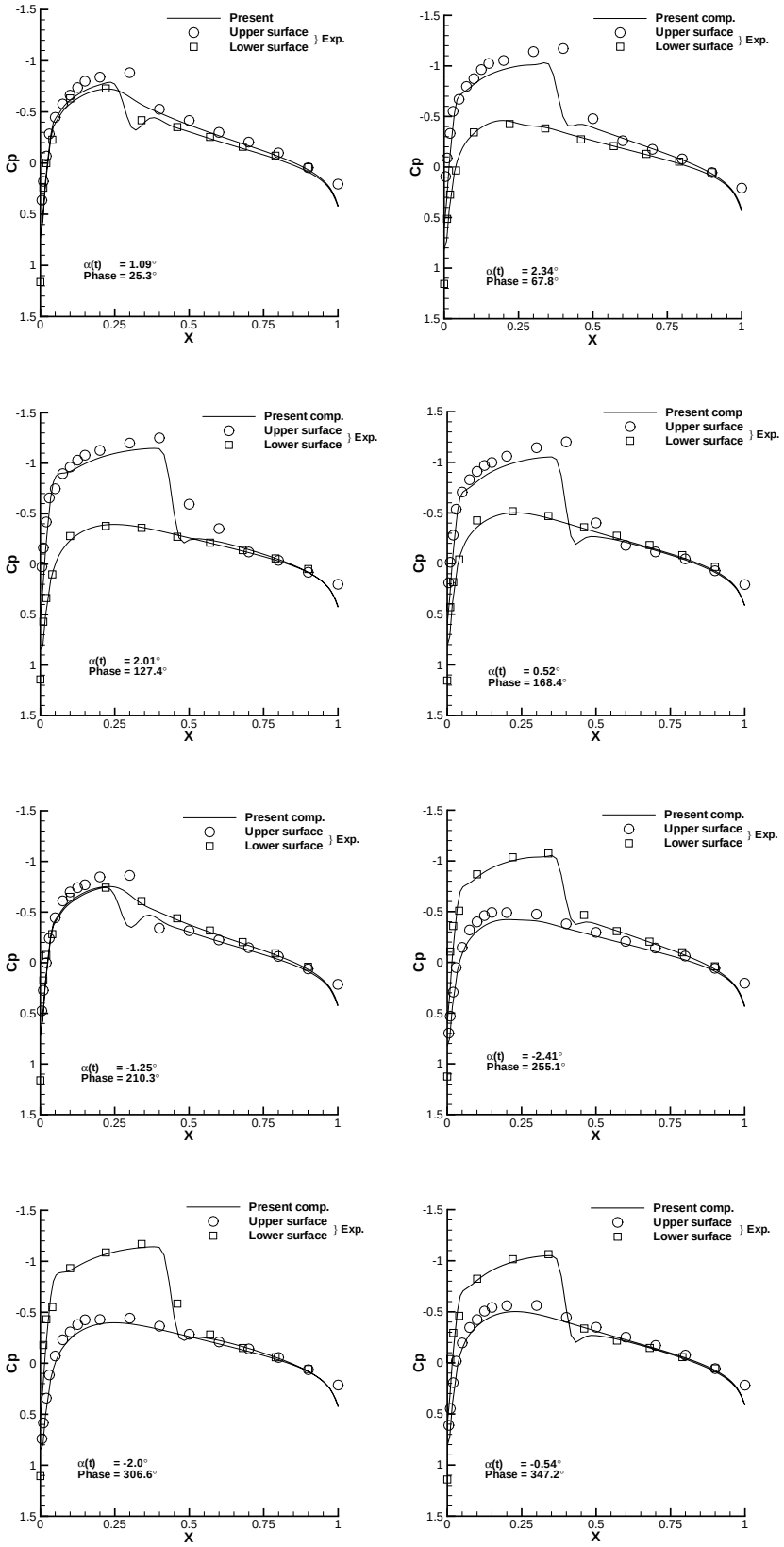

Fig. 12 Comparison of surface pressure distributions between present computation and experiment, NACA 0012, $M_\infty = 0.755$**,** $\alpha_m = 0.016\,\mathrm{deg}$**,** $\alpha_0 = 2.51\,\mathrm{deg}$**,** $\kappa = 0.0814$**.**

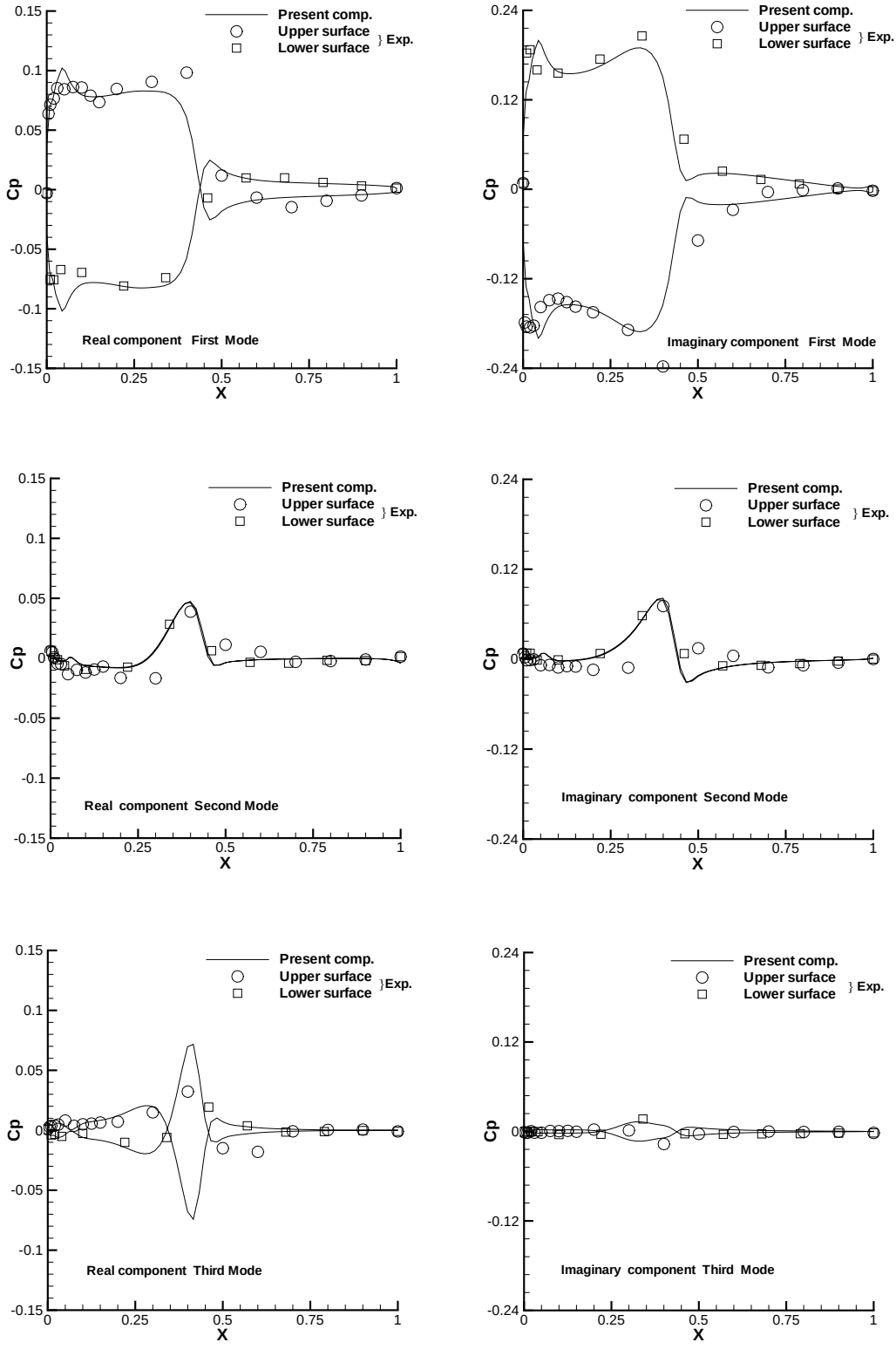

Fig. 13 Comparison of Fourier Components of surface pressure variations between present computation and experiment, NACA 0012, $M_\infty = 0.755$, $\alpha_m = 0.016\,\mathrm{deg}$, $\alpha_0 = 2.51\,\mathrm{deg}$, $\kappa = 0.0814$.

VII. Conclusions

This paper presents an efficient numerical method for solving the unsteady Euler equations on stationary Cartesian grids. It is shown that the boundary conditions on the surface of an airfoil can be approximated by their first-order expressions on the mean position of the airfoil chord while the full Euler equations are solved in the flow field on stationary non-body-conforming Cartesian type of grids. For steady transonic flows, the calculated pressure distributions, lift coefficients, wave drag coefficients, and pitching moment coefficients by the approximate method in general agree well with the solutions of FLO52 using body-conforming curvilinear grids for airfoils of thickness ratios up to 15% and angle of attack up to 8 degrees. For unsteady flows, the calculated instantaneous lift, moment, surface pressure distributions and the Fourier components of the surface pressure variations by the approximate method agree well with the experimental data for the NACA0012 airfoil with oscillating pitch angles up to 3 degrees at transonic speeds. There is no restriction on the size of the mean angle of attack. The advantage of using a single stationary non-body-conforming rectilinear grid opens the door for the efficient computation of unsteady fluid-structure interaction problems involving small unsteadily deforming airfoils or wings of small thickness by using the present approximate boundary-condition method.

Acknowledgement

This work has been supported by NASA Langley Research Center, contract number NAG-1-02050.

References

[1]Rodden, W. P. and Johnson, E. H., *MSC/NASTRAN Aeroelastic Analysis User's Guide, Version 68*, The Macneal-Schwender Corporation, Los Angeles, 1994.

[2]Lee-Rausch, E. M. and Batina, J. T., "Wing Flutter Boundary Prediction Using Unsteady Euler Aerodynamic Method," *Journal of Aircraft*, Vol. 32, No. 2, Mar.-Apr. 1995, pp. 416–422.

[3]Lee-Rausch, E. M. and Batina, J. T., "Wing Flutter Computations Using an Aerodynamic Model Based on the Navier-Stokes Equations," *Journal of Aircraft*, Vol. 33, No. 6, Nov.-Dec. 1996, pp. 1139–1147.

[4]Liu, F., Cai, J., Zhu, Y., Wong, A. S. F., and Tsai, H.-M., "Calculation of Wing Flutter by a Coupled Fluid-Structure Method," *Journal of Aircraft*, Vol. 38, No. 2, Mar.-Apr. 2001, pp. 334–342.

[5]Gibbons, M., "Aeroelastice Calculations Using CFD for a Typical Business Jet Model," NASA CR 4753, 1996.

[6]Bartels, R., "Flow and Turbulence Modeling and Computation of Shock Buffet Onset for Conventional and Supercritical Airfoils," NASA TP 1998-206908, 1998.

[7]Tang, L., Bartels, R., Chen, P., and Liu, D. D., "Numerical Investigation of Transonic Limit Oscillations of a 2-D supercritical Wing," AIAA Paper 2001-1290, 2001.

[8]Batina, J. T., "A Finite-Difference Approximate-Factorization Algorithm for Solution of the Unsteady Transonic Small-Disturbance Equation," NASA TP 3129, Jan. 1992.

[9]Edwards, J., "Transonic Shock Oscillations Calculated with a New Interactive Boundary Layer Coupling Method," AIAA Paper 93-0777, 1993.

[10]Edwards, J., "Transonic Shock Oscillations and Wing Flutter Calculated with an Interactive Boundary Layer Coupling Method," Euromech-colloquium 349, simulation of fluid-structure interaction in aeronautics, gottingen, germany, Sept. 1996.

[11]Jameson, A., "Time dependent calculations using multigrid, with applications to unsteady flows past airfoils and wings," AIAA Paper 91–1596, June 1991, 10th AIAA Computational Fluid Dynamics Conference.

[12]Jameson, A., Schmidt, W., and Turkel, E., "Numerical Solutions of the Euler Equations by Finite Volume Methods Using Runge-Kutta Time-Stepping Schemes," AIAA Paper 81–1259, June 1981.

[13]Liu, F. and Ji, S., "Unsteady Flow Calculations with a Multigrid Navier-Stokes Method," *AIAA Journal*, Vol. 34, No. 10, Oct. 1996, pp. 2047–2053.

[14]Landon, R. H., "NACA 0012 Oscillating and Transient Pitching, Compendium of Unsteady Aerodynamic Measurements, Data Set 3," AGARD Report R-702, Aug. 1982.

[15]Batina, J. T., "Unsteady Euler Airfoil Solutions Using Unstructured Dynamic Meshes," *AIAA Journal*, Vol. 28, No. 8, Aug. 1990, pp. 1381–1388.